Since January 2020 Elsevier has created a COVID-19 resource centre with free information in English and Mandarin on the novel coronavirus COVID-19. The COVID-19 resource centre is hosted on Elsevier Connect, the company's public news and information website.

Genomics 112 (2020) 4863–4874

Contents lists available at ScienceDirect

Genomics

journal homepage: www.elsevier.com/locate/ygeno

G-quadruplex stabilization in the ions and maltose transporters gene inhibit *Salmonella enterica* growth and virulence

Neha Jain[a], Subodh Kumar Mishra[a], Uma Shankar[a], Ankit Jaiswal[a], Tarun Kumar Sharma[b], Prashant Kodgire[a], Amit Kumar[a,*]

[a] Discipline of Biosciences and Biomedical Engineering, Indian Institute of Technology Indore, Indore, Simrol, Indore 453552, India
[b] Translational Health Science and Technology Institute, Faridabad, Haryana 121001, India

ARTICLE INFO

Keywords:
G-quadruplex
Multi-drug resistance
Drug targets
G-quadruplex ligand
Acridine derivatives
Salmonella enterica

ABSTRACT

The G-quadruplex structure is a highly conserved drug target for preventing infection of several human pathogens. We tried to explore G-quadruplex forming motifs as promising drug targets in the genome of *Salmonella enterica* that causes enteric fever in humans. Herein, we report three highly conserved G-quadruplex motifs (SE-PGQ-1, 2, and 3) in the genome of *Salmonella enterica*. Bioinformatics analysis inferred the presence of SE-PGQ-1 in the regulatory region of *mgtA*, SE-PGQ-2 in ORF of *entA,* and SE-PGQ-3 in the promoter region of *malE* and *malK* genes. The G-quadruplex forming sequences were confirmed by biophysical and biomolecular techniques. Cellular studies affirm the inhibitory effect of G-quadruplex specific ligands on *Salmonella enterica* growth. Further, PCR inhibition, reporter based assay, and RT-qPCR assays emphasize the biological relevance of G-quadruplexes in these genes. Thus, this study confirmed the presence of G-quadruplex motifs in *Salmonella enterica* and characterized them as a promising drug target.

1. Introduction

Salmonella enterica belongs to the *Enterobacteriaceae family* and is known to cause typhoid fever and food poisoning. *Salmonella enterica* contains six subspecies among those, *S. enterica* is known to infect humans and further divided into two subclasses (Fig. 1a) [1,2]. Typhoidal class of *S. enterica* included *S. enterica* subsp. *enterica ser.* Typhi (*S.* ser. Typhi) and *S.* ser. Paratyphi and are known to causes typhoid fever, whereas non-typhoidal class includes *S.* ser. Enteritidis, and *S.* ser. Typhimurium causes food poisoning in humans [3]. As per the Centers for Disease Control and Prevention (CDC), typhoid fever causes ~22 million new cases and ~ 200,000 deaths every year across the world [4]. The emergence of anti-microbial resistance for chloramphenicol, co-trimoxazole, ampicillin, ciprofloxacin, ofloxacin, azithromycin, and cephalosporin leads to increased death rate due to clinical treatment failure and make the situation more dangerous [5–7]. Due to its high prevalence and rapid emergence of drug resistance, *Salmonella* rings a global alarm for the development of novel and promising therapeutic approaches.

S. enterica is an intracellular pathogen that grows in phagocytes and macrophages. During the growth phase, the host innate immune system generates various nitro-oxidative and oxidative stresses to eradicate this pathogen. However, *S. enterica* possesses a magnesium homeostasis mechanism that is mainly controlled by *mgtA gene* and helps bacteria to survive in nitro-oxidative stressed conditions [8]. The *mgtA* encodes for an Mg^{2+} transport ATPase that neutralizes the reactive nitrogen stress (RNS, nitro-oxidative) and plays a vital role in the bacterial survival inside macrophages (Supplementary data 1: Fig. S1a) [9]. Hence, targeting *mgtA* gene expression may serve as a promising therapeutic approach against *S. enterica* pathogenesis.

Similar to Mg^{2+}, Iron(Fe) is also an essential nutrient element for the *S. enterica*. The *S. enterica* contains an *entA*BCDEF operon that encodes for two low molecular weight siderophores (enterobactin and salmochelin) that have a high affinity for iron than the host iron-binding proteins and import iron inside the bacteria cell (Supplementary data 1: Fig. S1b) [10]. The formation of these siderophores involves the conversion of 2,3-dihydro-2,3-dihydroxybenzoate (2,3 DHB) to 2,3-dihydroxybenzoate (DHB) in the presence of 2,3-dihydro-2,3-dihydroxybenzoate dehydrogenase enzyme (EntA), that is encoded by *entA* of *entA*BCDEF operon. The inhibition of *entA* gene expression has been observed to abolish the DHB formation leading to the reduced production of enterobactin and salmochelin [11]. Targeting the production of siderophore has previously shown to have anti-microbial activity against *Mycobacterium tuberculosis* [12], *Aspergillus*

* Corresponding author at: Discipline of Biosciences and Biomedical Engineering, Indian Institute of Technology-Indore, Indore, Simrol, 453 552, India.
E-mail address: amitk@iiti.ac.in (A. Kumar).

https://doi.org/10.1016/j.ygeno.2020.09.010
Received 20 November 2019; Received in revised form 15 July 2020; Accepted 3 September 2020
Available online 06 September 2020

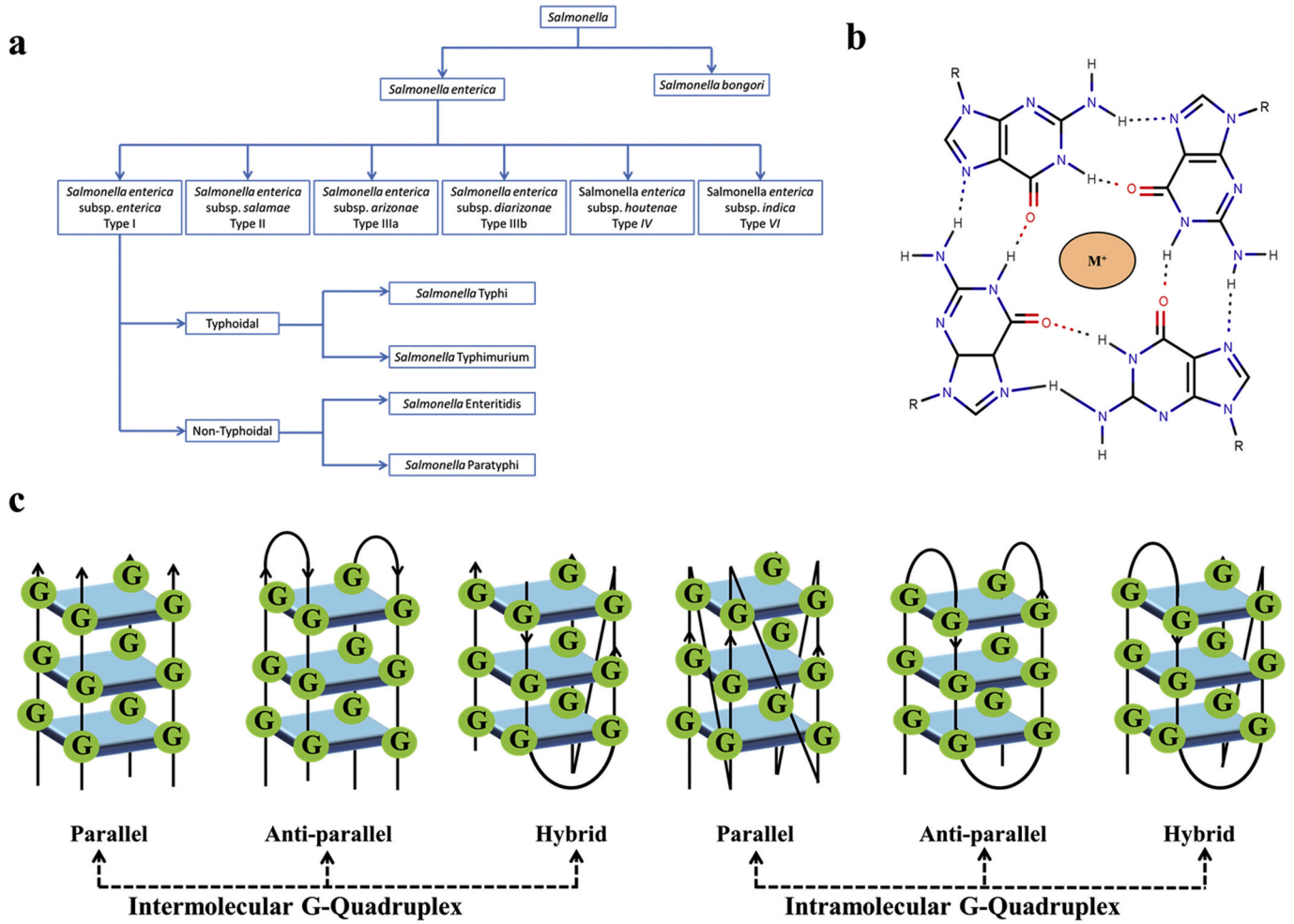

Fig. 1. *Salmonella* genus classification and G-quadruplex topologies. a) Flowchart depicting the classification of the *Salmonella* genus. b) G-quartet structure showing hoogsteen hydrogen bond formation between Guanines and cation binding. c) Different types of topologies formed by intermolecular and intramolecular G-quadruplex structures.

fumigatus [13], *Yersinia pestis* [14], *Pseudomonas aeruginosa* [15], and *Vibrio chloreae* [16]. Therefore, targeting *entA* gene may prove as another therapeutic approach to combat the infection and virulence of *S. enterica*.

Similar to magnesium and iron, maltose is another essential nutrient for the *S. enterica* that serves as a significant source of carbon for this bacterium. The uptake of maltose from the host environment is tightly regulated by two genes, *malK* and *malE* (Supplementary data 1: Fig. S1c) [17]. Inhibiting the *malK* and *malE* synthesis has shown to decline the growth of *S. enterica* [18]. Henceforth, targeting these three genes (*mgtA, entA*, *malK,* and *malE*) will make *S. enterica* unable to grow inside the gastrointestinal tract.

G-rich regions having a motif $G_{>2}N_LG_{\geq 2}N_LG_{\geq 2}N_LG_{\geq 2}$ present in the genome tends to form specific non-canonical secondary structures known as G-quadruplex (G4). These G4s are stabilized by the presence of monovalent and some divalent cations and can adopt various topologies (Fig. 1b & 1c) [19,20]. This structural diversity has been exploited for the diagnosis and therapeutic targeting [21,22]. The G-quadruplex structure forming nucleic acid motifs have been shown to be evolutionarily conserved in eukaryotes [23], prokaryotes [24], protista [25], plants [26] and viruses [27] and work as promising drug targets in various diseases such as cancer, neurological disease, and virus infection. The G4s are reported to play a regulatory role in various biological processes such as regulating DNA replication by the specification of origin of replication (ORI) sites, telomere maintenance in human cells, antigenic variations by regulating recombination, transcription, and translation.

Recently, G-quadruplexes are being investigated for their involvement in virulence and survival mechanisms of various human pathogens [28]. Stabilization of G4s in protozoans: *Plasmodium falciparum, Trypanosoma brucei* and *Leishmania donovani* have shown anti-protozoal activities [29]. Further, G4s have emerged as a promising drug target in viruses like SARS coronavirus, Human Papilloma virus (HPV), Zika, Ebola, Herpes simplex virus (HSV), Epstein-Barr virus (EBV), Hepatitis B virus (HBV), Hepatitis C virus (HCV), Human immunodeficiency virus 1 (HIV-1), Nipah virus, Adenoviruses, etc. where they play an essential role in proliferation and pathogenicity [27,30,31]. In bacteria, G4 present at the upstream of *pilE* locus, *B31 vlsE* locus and *tprK* antigen protein in *Neisseria gonorrhoea*, *Borrelia burgdorferi,* and *Treponema pallidum,* respectively acts as an activator for the initiation of antigenic variation and helps the pathogens in bypassing the immune system of the host [28]. In *Deinococcus radiodurans*, G4 sequences present in the regulatory regions of various genes contribute to radioresistance [32]. Similarly, G4 present at the upstream of *nasT* in *Paracoccus denitrificans* is involved in nitrite assimilation [33].

All these reports demonstrate the pivotal role of G-quadruplex in human pathogens, and their conserved-ness suggests them as a promising drug target for both drug-susceptible and drug-resistant strains of pathogens. Therefore, a comprehensive study that discovers highly conserved G-quadruplex in the essential genes of *S. enterica* may provide a more suitable therapeutic approach for fighting against infection and overcome the emergence of the drug-resistant problem in this deadly pathogen.

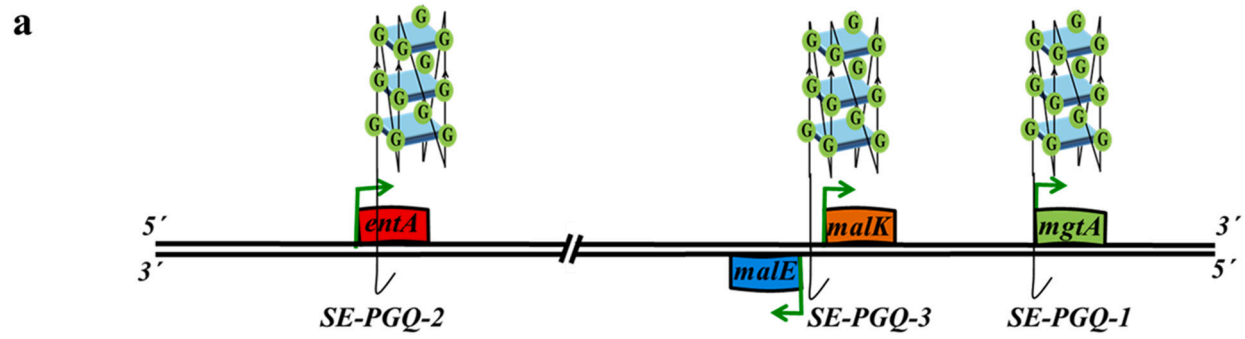

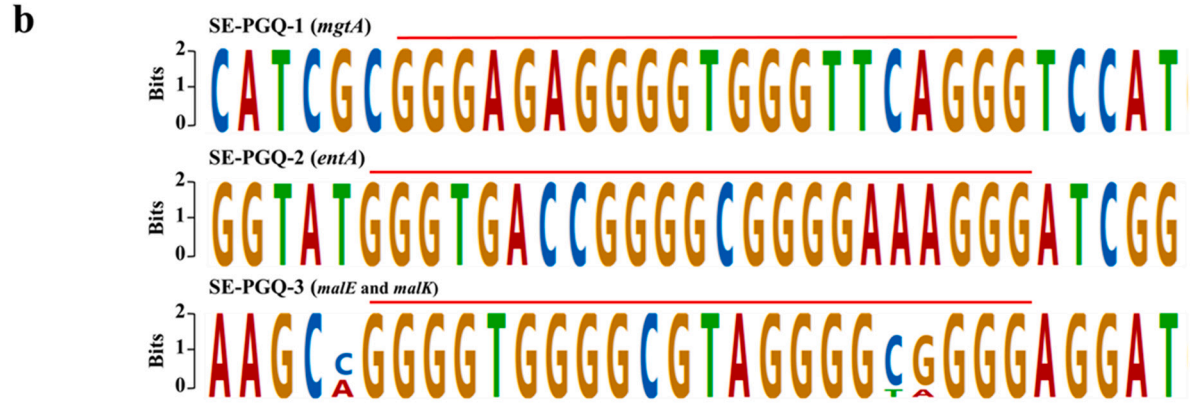

c

# PGQs	G4 Sequences	Conserved ness	Gene ID	Start	End	G4 Strand	Associated Functions	Gene Direction
SE-PGQ-1 *(mgtA)*	GGGAGAGGGGTGGGTTCAGGG	96 %	1250998	4655597	4655577	Antisense	Magnesium-translocating P-type ATPase mgtA (169bp upstream)	>>>>
SE-PGQ-2 *(entA)*	GGGTGACCGGGGCGGGGAAAGGG	98 %	1247106	644073	644095	Sense	2,3-dihydro-2,3-dihydroxybenzoate dehydrogenase (entA)	>>>>
SE-PGQ-3 (*malE* and *malK*)	GGGGTGGGGCGTAGGGGCGGGG	98%	*malE*-1250642 *malK* 1250643	4295743	4295722	Antisense	Intergenic region between maltose/maltodextrin ABC transporter substrate-binding protein *malE* (103 bp upstream) and maltose/maltodextrin import ATP-binding protein *malK* (259 bp upstream)	*malE* <<<< *malK* >>>>

Fig. 2. Representation and localization of three highly conserved PGQs. a) Diagrammatic representation of SE-PGQ-1 harbored at upstream of *mgtA*, SE-PGQ-2 in the open reading frame of *entA gene,* and SE-PGQ-3 in the intergenic regulatory region of *malK* and *malE* in the *Salmonella enterica* genome. b) Details of three most conserved PGQs, including location, Gene id, Gene locus, G-quadruplex strand, and gene direction in the reference genome of *Salmonella enterica* (CT18 strain). c) Consensus Sequence of the most conserved PGQs predicted by Glam2 tool of MEME Suite.

In the present study, we sought to explore the highly conserved potential G-quadruplex forming sequences (SE-PGQs) in completely sequenced strains of *S. enterica*. Bioinformatics analysis revealed the presence of three SE-PGQs in three different gene locations of *S. enterica* genome. SE-PGQ-1 was found to be present in the regulatory region of *mgtA*, SE-PGQ-2 in the open reading frame of *entA,* whereas SE-PGQ-3 in the regulatory regions of *malK* and *malE* genes (Fig. 2a). In order to confirm the formation of G-quadruplex structure by SE-PGQs, CD, NMR, and EMSA were employed and to validate these SE-PGQs as a potential drug target, CD melting, and polymerase stop assays were performed. Disc diffusion assay and MTT assay confirmed the growth inhibition of *S. enterica* cells by G4 binders BRACO-19 (9-[4-(*N*,*N*-dimethylamino) phenylamino]-3,6-bis(3-pyrrolodinopropionamido) acridine) and 9-Aminoacridine. Further, Real-time PCR (RT-PCR) revealed the reduced expression of genes that harbor these SE-PGQs in either their coding region or regulatory region upon the treatment with both BRACO-19 and 9-Aminoacridine. mTFP reporter based assay further strengthens the role of SE-PGQs in the gene expression regulation. This change in expression of PGQ harboring genes in the presence of G4 binding ligand suggested a G4 mediated regulatory mechanism in the expression of these genes. Therefore, G-quadruplex motifs found in these genes can be utilized as a potential drug target to develop a promising anti-microbial therapeutics. Moreover, the high conserved-ness of these SE-PGQs, even in the drug-resistant strain would be able to overcome the problem of the emergence of drug-resistance in *S. enterica.*

2. Result and discussion

2.1. Salmonella enterica genome harbors three most conserved G-quadruplexes

Since the last several decades, the scientific community has been witnessed a rapid increase in the number of such human pathogenic bacterial species that acquired resistance to multiple anti-bacterial agents. Currently, the emergence of multidrug-resistant strains remains a significant public health concern for clinical investigators that rings a global alarm to search for novel and highly conserved drug targets. Recently, conserved G-quadruplexes and their binding with small molecules are being extensively investigated as a promising therapeutic approach for combating the various type of human pathogenic infection [27,28]. Considering the suitability of G-quadruplex structure as a promising drug target in both drug-susceptible and drug-resistant strains of pathogens, here we sought to search for G-quadruplex motifs in *S. enterica* strains.

Comprehensive mining of potential G-quadruplex forming motifs (SE-PGQs) was performed on 412 completely sequenced strains of *S. enterica* (Supplementary data 1: Table S1). The bioinformatics analysis observed a total of 109,400 PGQs in 412 strains of *S. enterica* (Supplementary Dataset 2). Given that, a similar sequence may correspond to the same structure and evolutionarily conserved function, all the predicted PGQs were further clustered by Unweighted Pair Group Method with Arithmetic Mean clustering method using Clustal Omega tool. The conserved-ness is an essential parameter that makes these PGQ motifs suitable to work as promising drug targets. Therefore, next, we examined the conservation of each PGQ clustered using the following equation:

$$p = (n \div N) \times 100$$

where p is the frequency of occurrence, n = number of strains with specific G4 sequence, and N represents the total number of strains of *S. enterica.* These conservation analysis revealed 187 PGQ clusters that were observed to possess conversed-ness in more than 90% strains of *S. enterica* (Supplementary data 1: Table S2). G-quadruplex with loop length 1–7 and G tract of ≥3 forms a more stable G-quadruplex [34]. Therefore, for further study, we selected only those PGQs that satisfied the aforesaid criteria of G-quadruplex formation and were listed in Supplementary data 1: Table S3.

These predictions were further crosschecked with QGRS Mapper and PQSFinder (Supplementary data 1: Table S4 and S5). Interestingly, out of 18 PGQ clusters, three PGQs (SE-PGQ-1, SE-PGQ-2, and SE-PGQ-3) were found to be conserved in more than 98% strains of *S. enterica* (Supplementary data 1: Table S3) and present in the four essential genes namely *mgtA*, *entA*, *malK* and *malE* (Fig. 2a-c). The consensus sequence depicted the conserved Guanine residues of SE-PGQ motifs during the evolutionary process (Fig. 2b).

2.2. *In vitro* ^{1}H NMR analysis affirms the formation of G-quadruplex in SE-PGQs

NMR spectroscopy is considered as the most reliable technique for confirming the formation of G-quadruplex structure formation by the nucleic acid sequences. Therefore 1D ^{1}H NMR spectroscopy was performed to confirm the formation of G-quadruplex conformation by SE-PGQs. The presence of a chemical shift in the range of 10–12 ppm in 1D ^{1}H NMR spectra depicts the presence of hoogsteen base pairing in characteristic G-tetrads of G-quadruplex structure whereas, canonical G-C Watson Crick base pairing can be characterized by a chemical shift in the range of 12–14 ppm. All the three SE-PGQs showed an imino proton resonance between 10 and 12 ppm and clearly affirmed the formation of G-quadruplex structure (Fig. 3 and Supplementary data 1: Fig. S2). Whereas, mutant sequence NMR spectra analysis depicted an absence of imino proton peaks between 10 and 12 ppm. (Supplementary data 1: Fig. S3).

2.3. Evaluating the topology and stability of the PGQs using circular dichroism

Circular dichroism is one of the widely used techniques for analyzing the topology of the G-quadruplex structure. G-quadruplex, depending upon its sequence, loop length, and bound cation, can form either a parallel, anti-parallel or hybrid conformation. A positive peak at ~260 nm and a negative peak at ~240 nm signifies for parallel G-quadruplex topology. However, a positive peak at ~290 nm and a negative peak at ~260 nm signifies for anti-parallel G-quadruplex topology. Two positive peaks at 260 nm and 290 nm with a negative peak at 240 nm depicts the mix or hybrid topology. Additionally, all the G-quadruplex conformers forms a positive peak at 210 nm [35]. Different cation affects the stability of the G-quadruplex structure to a different extent. The stabilizing ability of some well studied cations is ranked as follows: $K^+ > Na^+ > Mg^{2+} > Li^+$ [20]. Therefore, we performed the CD spectroscopy of SE-PGQs in these four different cations (K^+, Na^+, Li^+, and Mg^{2+}) containing buffers (Fig. 4 and Supplementary data 1: Fig. S4).

CD spectra analysis revealed the predominant parallel G-quadruplex topology exhibited by SE-PGQ-1 and SE-PGQ-3 in the presence of the K^+ ion, whereas SE-PGQ-2 showed hybrid G-quadruplex topology (Fig. 4a). As expected, CD spectral scanning performed in the increasing concentration of K^+ ion showed the maximum molar ellipticity in the highest K^+ ion concentration (Supplementary data 1: Fig. S5). Fig. 4b shows the CD melting curve of SE-PGQs in various cation conditions. CD melting analysis revealed the higher stability of the SE-PGQs in the K^+ ion concentration (Fig. 4b & c). To evaluate the significance of G-tracts for their G-quadruplex forming ability, the central Guanine was mutated to Adenine, and CD spectra analysis was performed in 50 mM K^+ ion (Supplementary data 1: Table S6). Mutants (mut-PGQ-1, mut-PGQ-2, and mut-PGQ-3) failed to show the characteristic CD signal of G-quadruplex i.e., a positive band at 210/260/290 nm and a negative band at 240 nm suggesting the mutation in G tract disrupted the G-quadruplex formation (Fig. 4a).

2.4. Electrophoretic mobility shift assay (EMSA) supports intramolecular conformations of SE-PGQs

Next, Electrophoretic Mobility Shift assay (EMSA) was performed to check the molecularity (inter or intra molecular G-quadruplex) of SE-PGQs in the solution. An intramolecular G-quadruplexes possess a compact topology and migrate faster than their linear counterpart, whereas intermolecular G-quadruplex contains a comparatively wider topology and exhibited slow migration than their linear counterpart [36]. All three SE-PGQs and positive control (Tel22 DNA G-quadruplex) showed faster mobility than their respective linear counterpart. They, therefore, suggested the formation of intramolecular G-quadruplex by SE-PGQs (Supplementary data 1: Fig. S6).

2.5. G-quadruplex specific ligands inhibit Salmonella enterica growth

Similar to the G-quadruplex motif present in the genome of another human pathogen, a G-quadruplex motif present in *mgtA*, *malK*, *malE, and entA* genes of *S. enterica* strains may also serve as a potential target for developing anti-bacterial therapy. These G-rich targets can also overcome the problem of the drug resistance due to their high conserved-ness in both drug-susceptible and drug-resistant bacterial strains. Recently, conserved G-quadruplexes and their binding with small molecules are being extensively investigated as a promising therapeutic approach for combating the various type of human pathogen infection [27,28]. For example, HIV-1 promoter region possessed a G-quadruplex motif in the long terminal repeat (LTR) region of their genome and observed to be critical for its proliferation. BRACO-19, a tri-substituted Acridine derivative, has shown anti-HIV-1 activity by stabilizing the G-quadruplex motif present in the LTR region [27]. BRACO-19 is also reported to inhibit the viral multiplication in Adenoviruses and Herpes Simplex virus by stabilizing G-quadruplex motifs in their genome [30,37].

Similarly, stabilization of G-quadruplex structure present in the core gene of HCV genome by PDP, halts its replication, translation and, therefore, can be used as potential anti-hepatitis therapeutics [38]. Pyridostatin is also observed to stabilize the G-quadruplex structure formed in the mRNA of the nuclear antigen 1 protein of EBV, leading to its translation suppression [39]. Recently, BRACO-19 has shown an inhibitory effect on *Mycobacterium tuberculosis,* and *Klebsiella pneumoniae,* while Quarfloxin inhibited *Plasmodium falciparum,* by stabilizing G-quadruplexes present in various regions of their genome [25,40,41]. Previously, 9-Aminoacridine and its derivatives have been observed for their anti-proliferative properties in cancer cells [42] by binding to the telomeric region [43], the *c-Myc* gene [44] and *c-Kit* promoter [45]. Therefore, here we analyzed the effect of G-quadruplex specific ligands, BRACO-19, and 9-Aminoacridine on the *S. enterica* growth and performed MTT assay. An increase in color intensity with the decrease in the concentration of G4 specific ligands was observed giving maximum

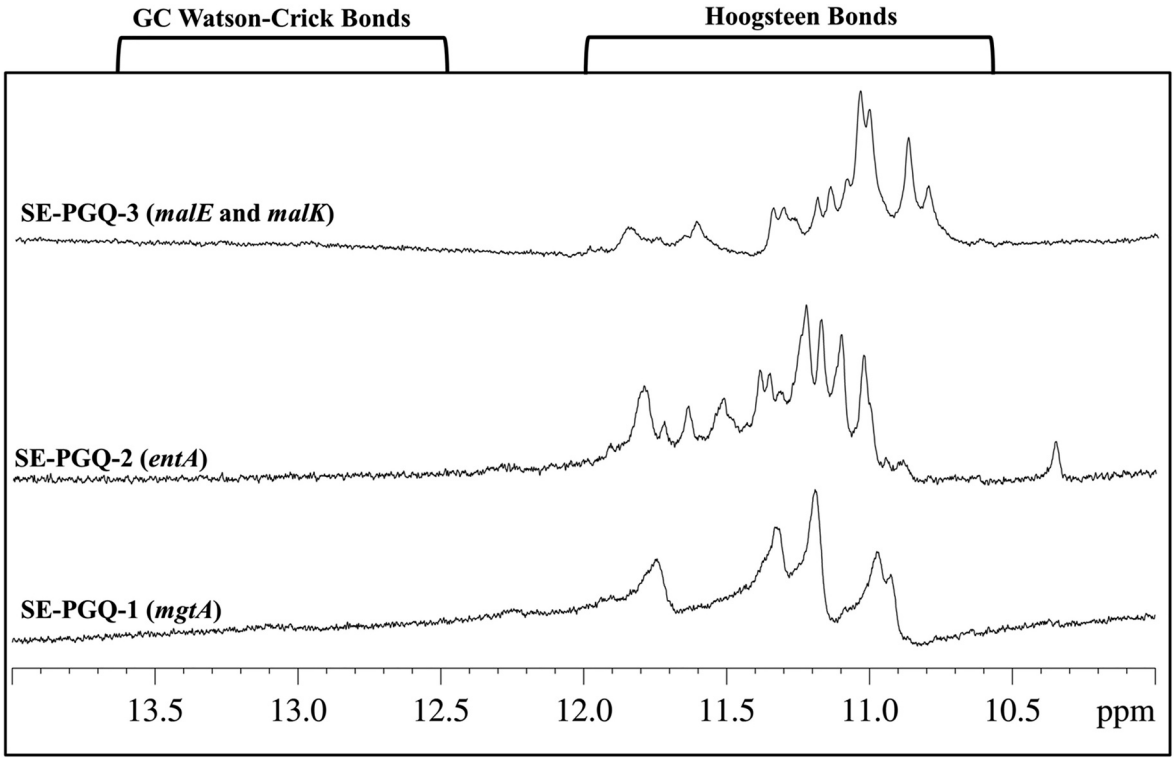

Fig. 3. NMR Spectra. 1D ^{1}H NMR spectra of SE-PGQ-1(*mgtA*), SE-PGQ-2(*entA*), SE-PGQ-3(*malE* and *malK*) in the presence of K^{+} Buffer.

in control well (untreated) that suggested the inhibitory effect of both G4 ligands, BRACO-19 and 9-Aminoacridine on the *S. enterica* growth with an IC_{50} value of 15.877 μM and 10.5 μM respectively (Supplementary data 1: Fig. S7 and S8).

2.6. Acridine derivatives have a higher affinity towards Salmonella enterica PGQs

Isothermal titration calorimetry (ITC) is one of the most reliable techniques for molecular interaction analysis as it relies on the change in enthalpy (ΔH) and entropy (ΔS) upon the interaction between two molecules. Herein, to check the specificity and affinity of BRACO-19 and 9-Aminoacridine with the SE-PGQs, we performed the ITC experiment in 50 mM potassium phosphate buffer and fitted the obtained thermogram in the two-site binding model (Fig. 5 and Supplementary data 1: Fig. S9). A duplex DNA was taken as a control. Negative change in free Gibbs energy (ΔG) depicted the thermodynamically favorable interaction between BRACO-19/9-Aminoacrdine and SE-PGQs and thus the formation of a stable complex. Briefly, in the interaction analysis of SE-PGQs with BRACO-19, ΔH was observed to be -6.88×10^{3} cal/mol, 4.49×10^{6} cal/mol, and 3.14×10^{2} cal/mol for SE-PGQ-1, SE-PGQ-2, and SE-PGQ-3 respectively. Negative ΔH for SE-PGQ-1 depicted that the reactions were enthalpy driven. Though SE-PGQ-2 and SE-PGQ-3 on interaction with BRACO-19 showed positive ΔH, a negative change in ΔG for both the reactions strengthens there biologically feasibility and were entropically driven. The first association constant (K_a1) for BRACO-19 was found to be $7.78 \times 10^{5}\ M^{-1}$, $2.73 \times 10^{6}\ M^{-1}$, and $9.37 \times 10^{5}\ M^{-1}$ for SE-PGQ-1, SE-PGQ-2, and SE-PGQ-3 respectively, which was 27.20, 95.5 and 32.76 folds higher than the duplex DNA ($2.86 \times 10^{4}\ M^{-1}$) [Fig. 5 and Supplementary data: Table S7] Similarly, with 9-Aminoacridine, the association constant for SE-PGQ-1, SE-PGQ-2 and SE-PGQ-3 was $-2.55 \times 10^{5}\ M^{-1}$, $-2.11 \times 10^{4}\ M^{-1}$, and $-2.48 \times 10^{5}\ M^{-1}$respectively and were enthalpy driven (Supplementary data 1: Table S8). For 9-Aminoacridine, the association constant (K_a1) was found to be 61.99, 52.02, and 62.98 folds higher for SE-PGQ-1, SE-PGQ-2, and SE-PGQ-3 respectively than the association constant for the negative control duplex DNA (Supplementary data 1: Fig. S10 and Table S8). On comparative analysis, it was observed that the BRACO-19 showed the highest affinity for SE-PGQ-2 ($2.73 \times 10^{6}\ M^{-1}$) while 9-Aminoacridine showed the highest binding against SE-PGQ-2 ($2.81 \times 10^{6}\ M^{-1}$). In summary, ITC analysis depicted the higher affinity and specificity of BRACO-19 and 9-Aminoacridine with SE-PGQs as compared to that of the duplex DNA [46,47].

2.7. Acridine derivative stabilizes the SE-PGQs, and thereby stalled the movement of polymerase

To understand the role of SE-PGQs in the cytotoxic effect of acridine derivatives, binding affinity of BRACO-19 and 9-amino acridine with these SE-PGQs were analyzed by performing CD Melting studies. An increase in the melting temperature (ΔT_m) was observed upon the addition of BRACO-19 compared with alone SE-PGQs (Fig. 6a). This indicated that BRACO-19 increased the thermodynamic stability of SE-PGQs (Fig. 6a). To check the stabilizing effect of BRACO-19 on the non G-quadruplex motifs, CD melting analysis was also performed on SE-PGQ-mutant sequences. The addition of BRACO-19 leads to a slight change in the T_m of the mutant sequences, depicting the higher affinity and stabilizing effect of BRACO-19 with SE-PGQ sequences as compared to that of their mutants. (Supplementary data 1: Fig. S10), CD melting analysis with 9-Aminoacridine was in line with that of BRACO-19 (Supplementary data 1: Fig. S11a). Further, we employed a PCR stop assay to investigate whether acridine derivatives complex formation with SE-PGQs, makes it possible to stop the movement of polymerase replication machinery or not. In order to investigate this hypothesis, we incubated PCR reaction mixture with BRACO-19 / 9-Aminoacridine in a concentration-dependent manner and then performed PCR amplification. We observed diminished intensity of bands with increase in concentration of acridine derivatives due to the formation of G-quadruplex motif leading to the unavailability of a template. However, in the absence of the BRACO-19 / 9-Aminoacridine, the band intensity was maximum indicated that the availability of template and Taq polymerase was able to extend the SE-PGQs motifs (Fig. 6b and Supplementary data 1: Fig. S11b). It shows that binding of the BRACO-19 and 9-Aminoacridine to

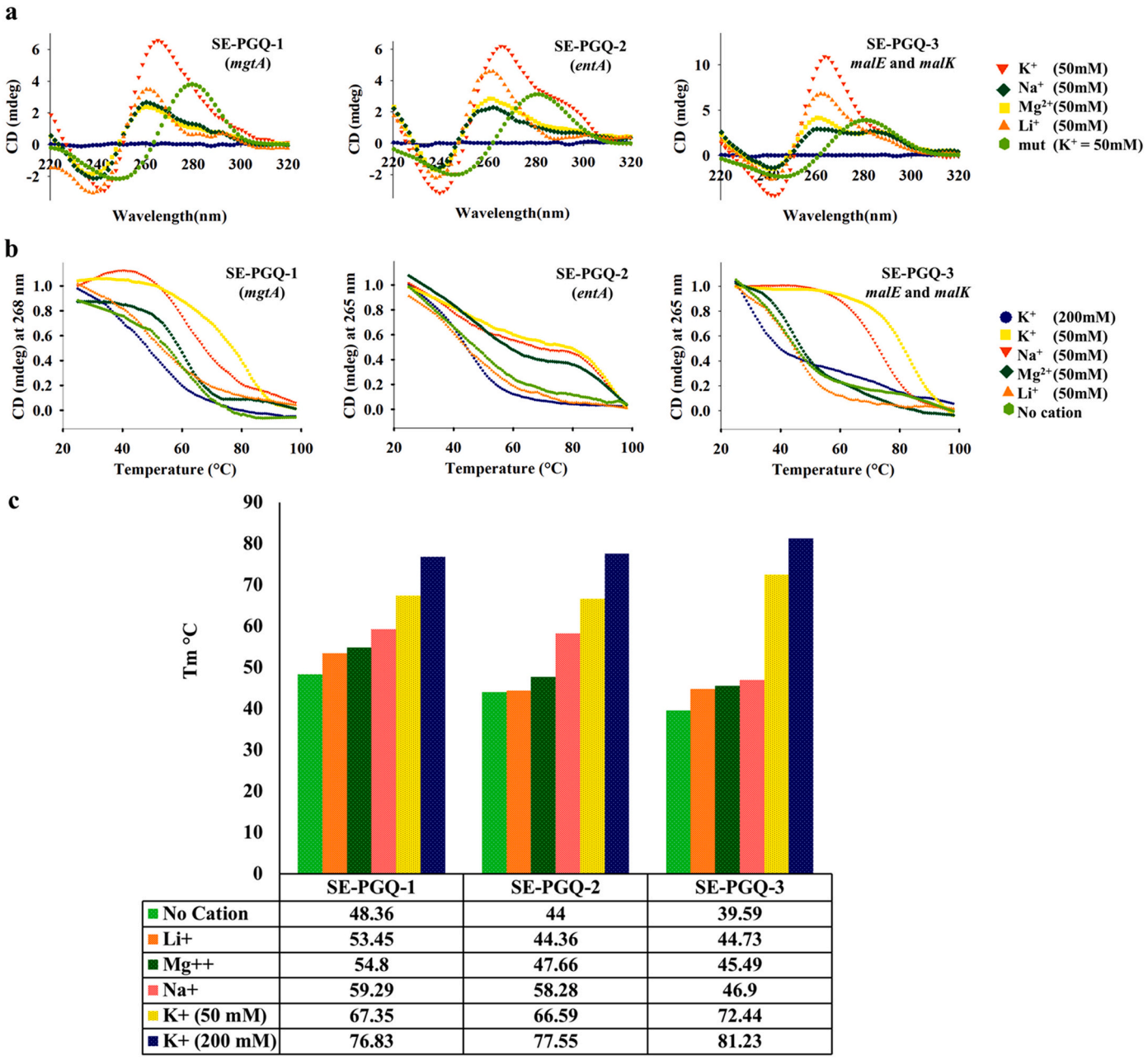

	SE-PGQ-1	SE-PGQ-2	SE-PGQ-3
No Cation	48.36	44	39.59
Li+	53.45	44.36	44.73
Mg++	54.8	47.66	45.49
Na+	59.29	58.28	46.9
K+ (50 mM)	67.35	66.59	72.44
K+ (200 mM)	76.83	77.55	81.23

Fig. 4. Circular Dichroism Analysis. a) Circular Dichroism spectra of the three most conserved PGQs in the presence of Tris-Cl buffer (10 mM) containing either of 50 mM K^+ (red), 50 mM Na^+ (green), 50 mM Li^+(yellow), 50 mM Mg^{2+} (blue) or mutant of the same length(Pink). b) Melting spectra obtained by Circular Dichroism in different buffers (K^+, Na^+, Li^+, and Mg^{2+}) for conserved PGQs predicted in *Salmonella enterica.* In the absence of any buffer(Black), K^+ 50 mM(Red), K^+ 200 mM (Green), Na^+ 50 mM (Yellow), Li^+ 50 mM (Blue)and Mg^{2+} − 50 mM (Pink). c) Bar-graph is depicting Tm of SE-PGQ-1(*mgtA*), SE-PGQ-2(*entA*), SE-PGQ-3(*malE,* and *malK*) in the absence and presence of various cations. (For interpretation of the references to color in this figure legend, the reader is referred to the web version of this article.)

the SE-PGQs motif stabilized the G-quadruplex structure and inhibited the movement of replication machinery over the untreated SE-PGQs. On the contrary, when mutant PGQs lacking G-tract were used as a DNA template, BRACO-19 and 9-Aminoacridine were not able to bind resulting in template availability and thus, could not inhibit the PCR amplification and produced a PCR product in the reaction(Fig. 6b and Supplementary data 1: Fig. S11b).

2.8. BRACO-19 inhibits the reporter gene expression by stabilizing the PGQ motifs

Highly stable G-quadruplexes in the regulatory regions and open reading frames of genes were previously shown to down-regulate the expression of genes [48–50]. Therefore, to analyze the effect of BRACO-19 on the translation of the harboring genes, mTFP based reporter assay was performed. The three SE-PGQ motifs were inserted in the open reading frame of teal fluorescence protein (mTFP) [Supplementary data 1: Fig. S12]. The plasmid was constructed with SE-PGQ motifs at the upstream of mTFP gene and transfected in HEK293 genes. On treating the transfected HEK293 with BRACO-19, a decrease in the fluorescence intensity was observed in comparison to the untreated cells depicting the stabilization of G4 motifs. An increase in the BRACO-19 concentration resulted in a further decrease of mTFP expression. This decrease in the mTFP expression shows the stabilization of G-quadruplex motifs by BRACO-19. The G4_mutant plasmid

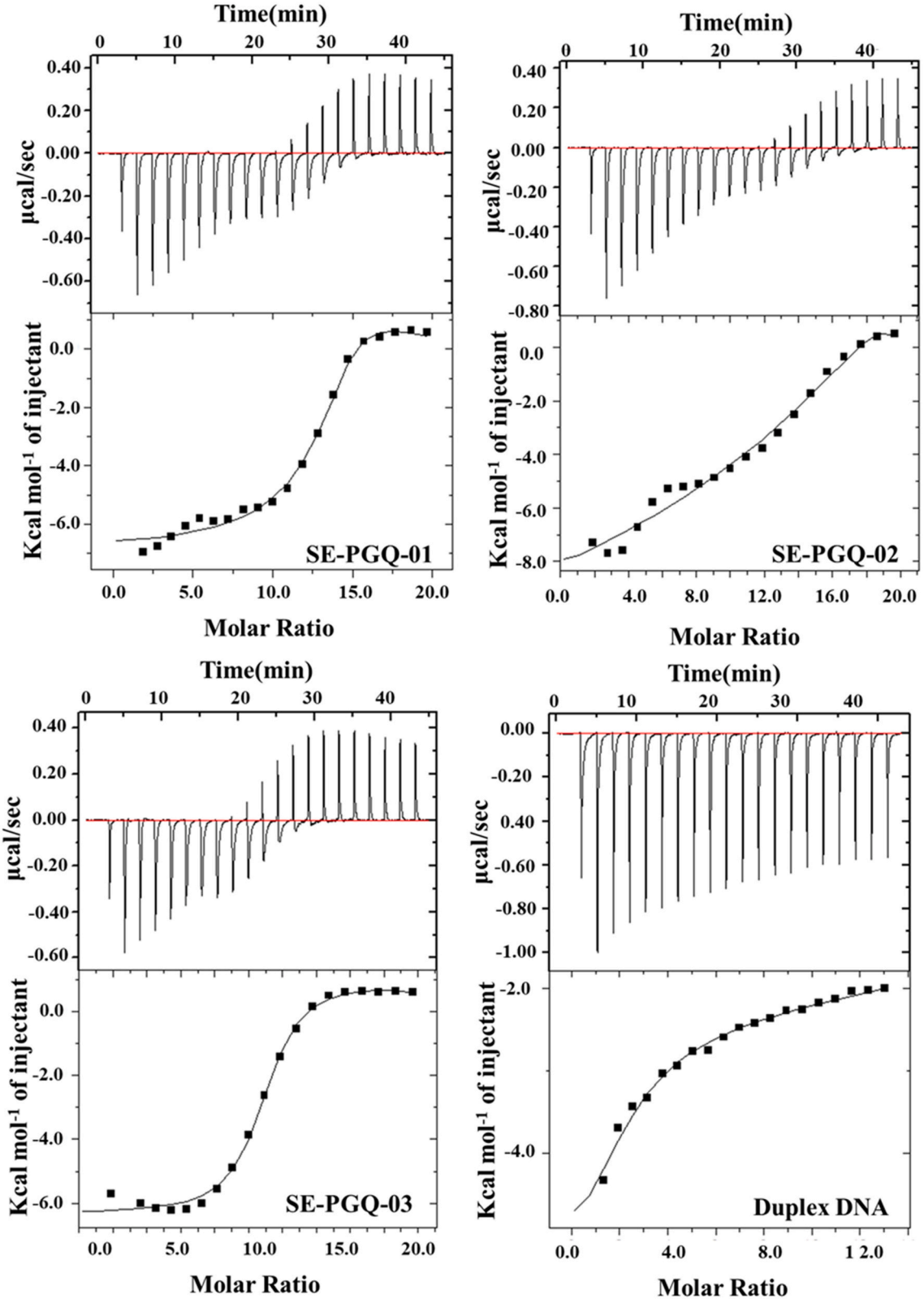

Fig. 5. ITC Analysis of SE-PGQs with BRACO-19. Isothermal titration calorimetry (ITC) binding isotherms for the interaction of BRACO-19 with SE-PGQ-1(*mgtA*), SE-PGQ-2(*entA*), SE-PGQ-3 (*malE* and *malK*) and Duplex DNA (Control). Raw data is shown in the upper panel and curve fit using a two-site binding model in the bottom panel. The graph represents one of the fitted curves out of the three repeats.

transfected HEK293 cells showed an almost similar level of mTFP expression in both treated and non-treated conditions depicting the G-quadruplex binding specificity of BRACO-19 (Supplementary data 1: Fig. S12).

2.9. 9-Aminoacridine and its derivative decrease the transcription rate of the genes harboring PGQs

Furthermore, we performed qRT-PCR assay to check the effect of

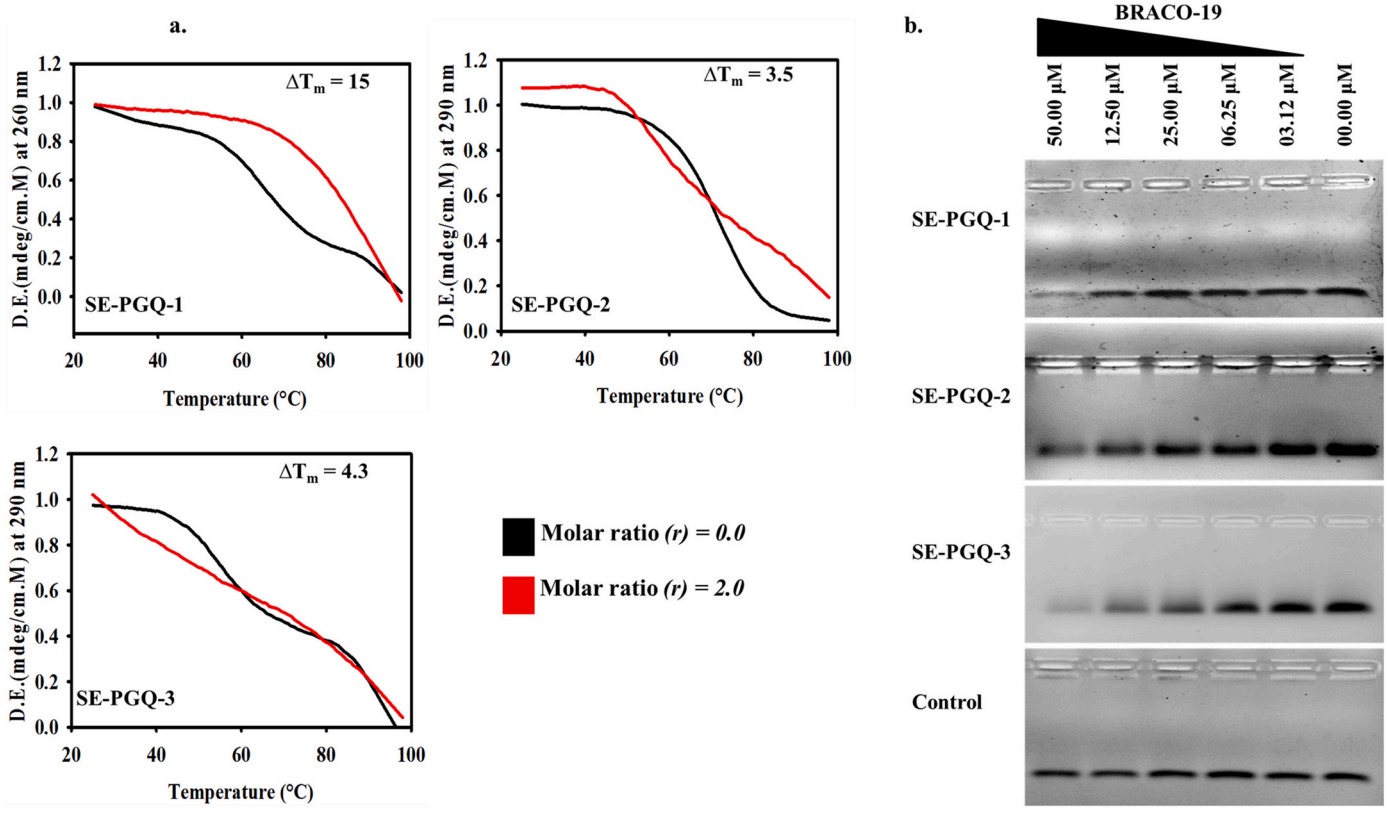

Fig. 6. Interaction of BRACO-19 with SE-PGQs. a) Circular Dichroism melting curve depicting the change in T_m of SE-PGQ-1 (*mgtA*), SE-PGQ-2 (*entA*), and SE-PGQ-3 (*malE* and *malK*) in the presence and absence of BRACO-19. b) Gel image of PCR stop assay for SE-PGQ-1(*mgtA*), SE-PGQ-2(*entA*), and SE-PGQ-3(*malE* and *malK*) and linear DNA with the increasing concentrations of BRACO-19.

BRACO-19 and 9-Aminoacridine on the expression of the PGQs harboring genes. The transcripts of the genes were quantified with respect to the 16 s rRNA gene, and the fold change in the expression of the transcripts was analyzed for the treated cells in comparison to non-treated cells (control culture). The samples treated with 15.877 μM BRACO-19 upon analysis showed 6.28, 3.42, 6.03, and 6.22 fold change in expression for *mgtA*, *entA*, *malE* and *malK,* respectively (Fig. 7). Similarly, the change in the gene expressions was also analyzed in the presence of another acridine derivative, 9-Aminoacridine. Inline with BRACO-19, 9-Aminoacridine reduced the rate of transcription of *mgtA*, *entA and malK* by 1.86, 3.03, and 2.94 fold, respectively (Supplementary data 1: Fig. S13). *malE* gene showed the highest suppression by 7.16 fold decrease in its expression in the presence of 9 amino acridine. In conclusion, all the four genes showed a decrease in the expression level, thus strengthening the G4 mediated inhibition mechanism in their promoter/regulator or open reading frame region (Fig. 7 and Supplementary data 1: Fig. S12).

Highly stable G-quadruplexes in the regulatory regions and open reading frames of genes were previously shown to down-regulate the expression of genes. The treatment of *S. enterica* cultures with Acridine derivatives, BRACO-19, and 9-Aminoacridine led to a decrease in the expression of *entA, mgtA, malK* and *malE genes*, suggesting a G-quadruplex mediated inhibition mechanism is involved in this process. As a schematic model elaborated in Fig. 8, G-quadruplex mediated inhibition of *entA, mgtA, malK,* and *malE genes* is expected to increase the innate immune response of host cells and reduced survival of bacterium inside the host cell. The Inhibited expression of the *entA and mgtA* proteins would make the bacteria unable to respond against Reactive oxygen/nitrogen (ROS/RNS)species and reduced their survival inside the host macrophages.

As a concluding remark, the current study shows the presence of stable and highly conserved G-quadruplex structures in essential genes of *Salmonella enterica*. The present study is a proof-of-concept analysis for the identification and characterization of G-quadruplex motifs in the

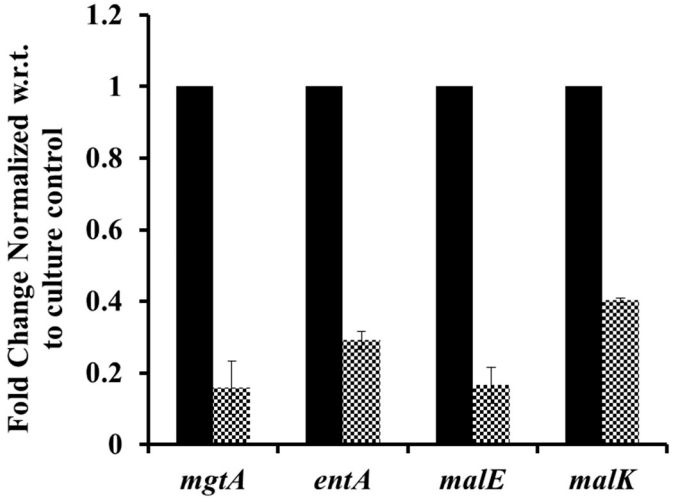

Fig. 7. RT-qPCR. The normalized fold change of *mgtA*, *entA*, *malE* and *malK* transcripts in *Salmonella enterica* determined by quantitative PCR in the presence of BRACO-19.

essential genes of *Salmonella enterica*. These SE-PGQs can provide a novel platform for therapeutic development against the infection of *Salmonella enterica*. They can be targeted in both antibiotic susceptible and antibiotic-resistant strains due to their conserved nature throughout the *Salmonella enterica* genus. Most of the commonly used G-quadruplex binders share a common structural feature of a planer hetero-aromatic chromophore that helps in π-π interaction with the G4 motif. A short alkyl chain substituents in this heterocyclic ring, usually terminated by an amino group, enhances the G4 specificity to a large extend [51]. 9-Aminoacridine satisfies this condition of the hetero-

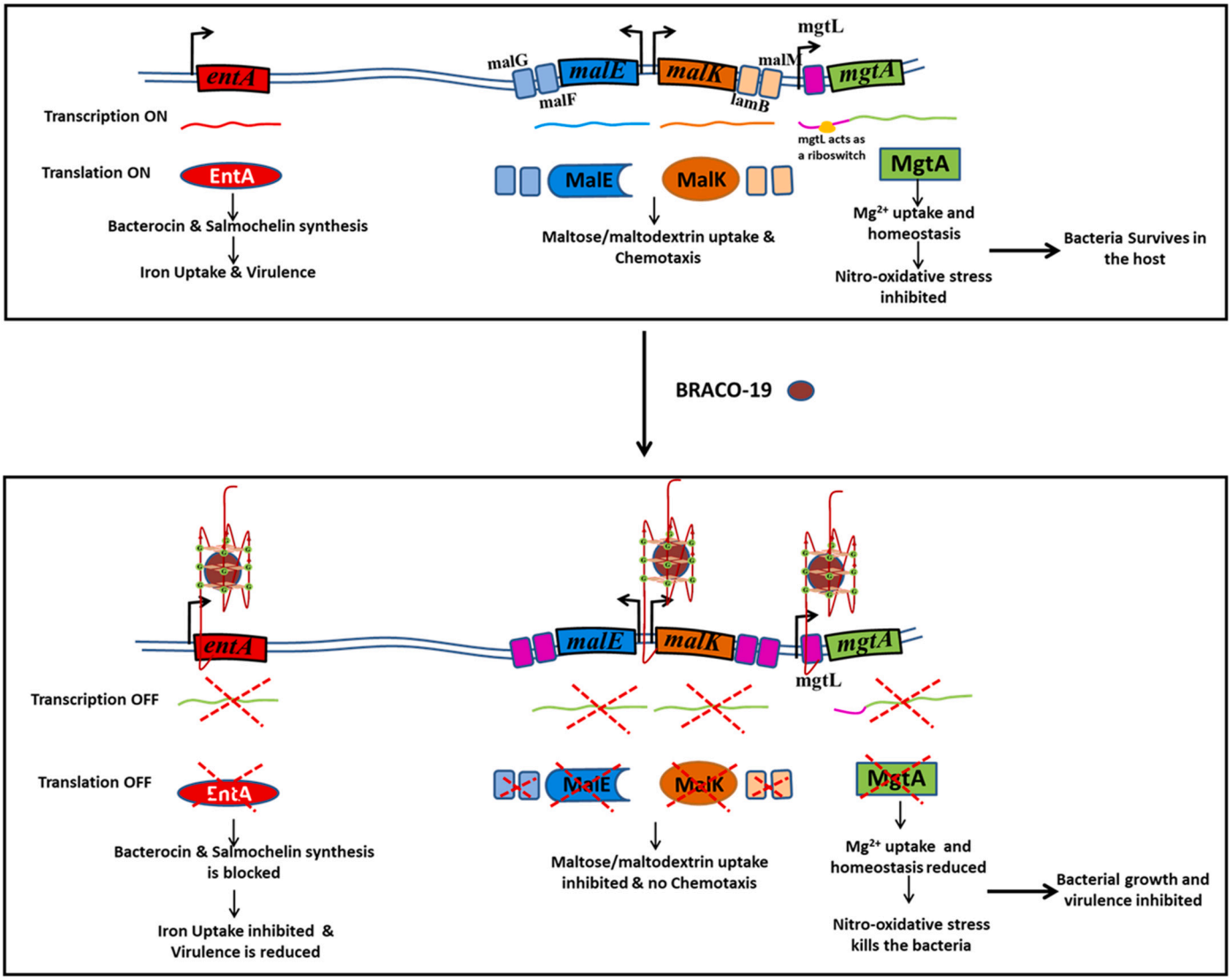

Fig. 8. Effect of Acridine derivatives on *mgtA*, *entA* and maltose operon mediated mechanisms. Schematic representation of G-quadruplex loci and the effect of their stabilization with BRACO-19 or 9-Aminoacridine on the survival and virulence of *Salmonella enterica*.

aromatic chromophore and can be substituted with the desired functional groups. This has been widely exploited for the synthesis of numerous di-substituted and tri-substituted Acridine Derivatives that have shown very high specificity towards G-quadruplexes as compared to the duplex DNA [42,43,45,52–58]. Thus, this Acridine scaffold can be used as a starting point for the synthesis of novel G4 specific ligands with minimum cytotoxicity to the host cells. Herein, two Acridine derivatives, BRACO-19 and 9-Aminoacridine were observed to bind and reduced the expression of these G-quadruplex structures possessing genes and thereby proposed as novel G4 mediated therapeutic approach for combating the infection of *Salmonella enterica* in humans.

3. Materials and methods

3.1. Prediction, conserved motif enrichment and functional analysis of G-quadruplex motifs in Salmonella enterica strains

Completely sequenced strains of *S. enterica* (Supplementary data 1: Table S1) were downloaded from National Center for Biotechnology Information (NCBI). These strains were then extensively mined for the potential G-quadruplex motifs in both sense and antisense strand using our previously developed G-quadruplex predictor tool [59]. This prediction tool used the following regular expression.

$$G_{\{T1\}}[X]_{\{L1\}}G_{\{T1\}}[X]_{\{L2\}}G_{\{T1\}}[X]_{\{L3\}}G_{\{T1\}}$$

where T1 represents consecutive tracts of Guanine that can be any number from 2 to 7, X is any nucleotide (A, T, G, C), L1, L2, L3 represents the variable loop region and can be any number from 1 to 20. For our prediction, we used G-tracts – 3 or 4 and loop length 1–20 nucleotide [59]. The results were further cross-verified by using QGRS Mapper [60] and PGSFinder [61] tools.

To find the conserved PGQ's that are available in all the strains, multiple sequence alignment (MSA) was performed by using Clustal Omega tool, and clustering was done using UPGMA method. Consensus sequences representing the whole G4 sequence with −5 and + 5 flanking regions were constructed using the Glam2 tool of MEME Suite [62].

The resultant PGQ clusters were then mapped for their gene location in the genome of the individual *S. enterica* strains using the coordinates extracted from our G4 prediction tool by using Graphics mode of GenBank Database (https://www.ncbi.nlm.nih.gov/nuccore/).

3.2. Salmonella genus G4 homolog prediction

In order to check the conservation of predicted PGQs at the *Salmonella* genus level, NCBI nucleotide BLAST was performed by taking each consensus PGQ as a query sequence and *Salmonella bongori*

genome sequences as a target (NCBI taxid: 590). The threshold e-value was set as 1e-3 to remove any results by chance.

3.3. Oligonucleotide preparation for CD and ITC analysis

Predicted G4 oligonucleotides sequences were procured from Sigma Aldrich Chemicals Ltd. (St. Louis, MO, USA). 100 μM stock solutions were prepared as per the manufacturer's instructions. Before each set of experiments, oligonucleotides were subjected to re-anneal by heating at 95 °C for 10 min and slow cooling at room temperature for 2 h. All these oligonucleotides were dissolved in four different Tris-buffer (pH = 7.0, 10 mM) containing 50 mM of K^+, Na^+, Li^+ and Mg^{2+} separately.

3.4. CD spectroscopy and melting analysis

CD experiments were performed for each oligonucleotide in different buffer conditions at 25 °C with a scanning rate of 20 nm/min from 220 to 320 nm using Jasco J-815 Spectropolarimeter (Jasco Hachioji, Tokyo, Japan). The instrument was equipped with a Peltier Junction temperature controller. Spectra were recorded in a cuvette of 1 mm path length for a final concentration of 20 μM of all oligonucleotides in Tris buffer (10 mM, pH = 7.4) containing four different cations viz. K^+, Na^+, Mg^{2+} and Li^+ (50 mM each) in separate experiments. To avoid signal contribution from the buffer, a blank spectrum containing only buffer was recorded before each measurement and subtracted from CD spectrum of the sample prepared in the respective buffer.

CD Melting analysis was performed for every PGQs (final concentration of 20 μM) with a temperature range of 25 °C to 98 °C in four different cations (K^+, Na^+, Mg^{2+} and Li^+, 50 mM each) containing buffers. The heating rate was set as 1 °C/min for each melting experiments

3.5. Electrophoretic mobility shift assay

Native PAGE was run using 20% polyacrylamide gel in 1× TBE buffer. Each sample was dissolved in Tris buffer(pH = 7, 10 mM) containing four different cations K^+, Na^+, Mg^{2+}, Li^+ (50 mM each) separately. For each PGQ, an oligonucleotide of similar length (G mutated with T nucleotide) was taken as a negative control, and standard G-quadruplex (Tel22 DNA) was taken as a positive control. 20 μL of each oligonucleotide sample were loaded, and electrophoresis was performed at 4^0C, 90 Voltage in a vertical gel unit system. The gels were visualized by staining with ethidium bromide and analyzed on ImageQuant LAS 4000 gel doc (GE Healthcare Biosciences Ltd., Sweden).).

3.6. One dimensional ^1H NMR spectroscopy

AVANCE 500 MHz BioSpin International AG, Switzerland equipped with a 5 mm broadband inverse probe was used to perform NMR spectroscopic analysis. The SE-PGQs were dissolved in 50 mM potassium phosphate buffer. All the NMR experiments were performed using H_2O/D_2O solvent at 9:1 ratio. Temperature of 298 K with 20 ppm spectral width and 3 - (Trimethylsilyl) propionic-2, 2, 3, 3-D4 acid sodium salt (TSP) as an internal reference were used. NMR data processing, integration, and analysis were done by using Topspin 3.1 software.

3.7. Isothermal titration calorimetric (ITC) analysis

ITC analysis was performed for all three PGQs and a linear DNA (negative control) using MicroCal iTC200 calorimeter (GE Healthcare, Biosciences Ltd., Sweden. All the oligonucleotides were dissolved in 50 mM potassium phosphate buffer at the final concentration of 20 μM. The oligonucleotide was used in the cell of ITC and 200 μM of 9-Aminoacridine and BRACO-19 dissolved in the same buffer were titrated 21 times by using syringe with the initial injection of 0.4 μL followed by 1.8 μL of the ligand at each step for the duration of 3.6 s with the decay of 90 s between each step. The heat of dilution of the oligonucleotides was determined by adding the same amount of 9-Aminoacridine/BRACO-19 into the 50 mM potassium buffer and was subsequently subtracted from the binding isotherms of the oligonucleotides before the curve fitting analysis. Data were acquired in triplicates and was analyzed or the determination of association constant by its two-site binding mode analysis using origin scientific software version 7 (Microcal Software Inc. Northampton, MA, USA).

3.8. Bacterial strain culture and growth conditions

The *S.* ser. Typhimurium strain ATCC 14028 was procured from HiMedia and streaked on Nutrient Agar (HiMedia). A single colony was inoculated in the in Nutrient Broth (HiMedia) and kept overnight at 37 °C and 220 rpm in the incubator shaker [63]..

3.9. MTT growth inhibition assay

MTT assay was performed for cytotoxic analysis of 9-Aminoacridine and BRACO-19 on *S. enterica*. 50 μL of the overnight grown culture of *S. enterica,* was inoculated in 5 mL Nutrient Broth (NB) at 220 rpm, 37 °C and allowed to grow till the $O.D_{600}$ = 0.5. After that, 50 μL was transferred in a fresh 5 ml NB tube, and 100 μL was transferred in each well of 96 well plates. Dilution was prepared from the stock solution (200 μM) of 9-Aminoacridine/BRACO-19 of the following concentrations 100 μM - 0.09 μM and added to the respective wells, last well served as blank (without 9-Aminoacridine). The plates were kept at 37 °C, 220 rpm for 3 h. Afterward, 10 μL of MTT (5 mg/mL) was added to each well and incubated for 3 h. Finally, 20 μL of DMSO was added in each well to dissolve formazan crystal, and the plate was examined using a microplate reader (BioTek) at 590 nm [64].

3.10. PCR stop assay

Templates and Primers were procured from Sigma-Aldrich Chemicals Ltd. (St. Louis, MO, USA) (Supplementary data 1: Table S9). The reaction was performed in the master mix consisting of 1× PCR buffer, 0.33 mM dNTPs, 2 μM templated, 2 μM reverse primer, 2.5 units Taq DNA polymerase (Sigma-Aldrich Chemicals Ltd. St. Louis, MO, USA) and dose titration of BRACO-19 and 9-Aminoacridine. The following thermal cycling conditions were used: initial denaturation at 95 °C for 5 min, followed by 25 cycles of 95 °C for 30 s, 50 °C for 30 s, 72 °C for 0.5 min and finally held at 4 °C. The 6× DNA loading dye was added to the amplified products and resolved in 3% agarose gel. Ethidium bromide was used for staining, and gel images were analyzed using ImageQuant LAS 4000 (GE Healthcare, Biosciences Ltd., Sweden).

3.11. mTFP reporter based assay

Reporter based assay was performed by utilizing a revised protocol described elsewhere [65]. Briefly, G-quadruplex harboring mTFP plasmid was constructed by inserting the G4 sequences and a mutant sequence just before the start codon of mTFP coding region in pCAG-mTFP plasmid [a generous gift from Dr. Debasis Nayak, IIT Indore]. Insertion was performed using an Overlap extension PCR based cloning strategy with overlapping forward and reverse primers. The constructed plasmids were transfected in HEK293 cell lines using Lipofectamine2000 as per the manufacturer's protocol. The transfected cells were incubated for 4 h, followed by the treatment of 10 μM and 20 μM BRACO-19. The treated cells were further incubated for 24 h and then visualized under Fluorescence microscope for mTFP expression analysis. ImageJ software was used for comparative intensity analysis.

3.12. Total RNA isolation and cDNA synthesis

S. enterica was grown overnight at 37 °C, 220 rpm in 5 mL of a test tube containing NB. Two flasks of 500 mL containing 50 mL of NB each

were inoculated with 1% inoculum from overnight culture. Both the flasks of untreated and treated cells were allowed to grow according to previously mentioned conditions till the $O.D_{600}$ nm reached 0.5. At $O.D_{600}$ = 0.5, 20 μM of BRACO-19 (dissolved in water) and 10.35 μM of 9-Aminoacridine (dissolved in DMSO) were added to MIC flask. For 9-Aminoacridine treatment assay, control culture DMSO was added as 9-Aminoacridine was dissolved in it. All the flasks were kept at 37 °C, 220 rpm for 45 min. Subsequently, samples were centrifuged at 12000 rpm and immediately preceded for RNA isolation. *S. enterica* culture prior to RNA isolation was treated with RNA protect reagent (Qiagen, USA) to stabilize RNA and prevent it from degradation. Treated and untreated *Salmonella* cultures were used for total RNA isolation. RNA isolation for all samples was carried out using TRIZOL reagent (Invitrogen) according to manufacturer's instructions. After RNA isolation, its concentration and purity were measured using NanoDrop (Thermoscientific) as ng/μL and A260/A280, respectively. Subsequently, all the RNA samples were treated with RNase-free DNaseI (Invitrogen) as mentioned by the manufacturer. Finally, 5 μg of total RNA from each sample was used for cDNA synthesis. cDNA synthesis was performed in a 20 μL reaction by using Invitrogen Superscript IV kit (Cat # 18091050) according to the manufacturer's instruction.

3.13. Gene expression profiling using real-time quantitative PCR

Quantitative Real-Time PCR was used to elucidate the variation in gene expression profiling of *Salmonella* treated with 9-Aminoacridine and BRACO-19. All the aliquots of cDNA from untreated (control) and treated (9-Aminoacridine/BRACO-19) were used in real-time PCR. qPCR was carried out in PCR master reaction mix containing 1× PowerUp™ SYBR® Green Master Mix (Applied Biosystem, USA), 0.5 μM of each primer and 11 μL of cDNA sample in a final reaction volume of 25 μL in a 96 well PCR plate in Step One Plus (Applied Biosystem, USA) Thermal Cycler. All the samples for real-time were analyzed in three dilutions and duplicates; normalization was done with respect to 16 s rRNA (housekeeping gene). The proportionate change in gene expression was assessed by change in expression of the target gene in treated as compared to control. List of primers used in real-time PCR and thermo-cycling conditions are mentioned in Supplementary data 1: Table S10 and S11, respectively. Briefly, the thermo-cycle used in qRT-PCR was 94 °C for 2 min, subsequently 40 cycles of 94 °C for 15 s and 57 °C for 1 min.

Authors contribution

Data conceptualization and methodology were performed by A.K. Bioinformatics analysis was done by N.J., and U.S. Biophysical analysis was performed by N.J., U.S.. N.J. and A.J. performed MTT assay. A.J., S.K.M. and N.J. performed RT-PCR under the supervision of P.K., and A.K.. N.J., and U.S. wrote the manuscript. A.K. T.K.S. and P.K. did the review and editing.

Funding

The work was supported by the Department of Science and Technology, Govt. of India [EMR/2016/3897 to AK], [EMR/2016/003547 to P.K.], and Department of Biotechnology, Govt. of India [BT/PR20319/BBE/117/189/2016 to P.K.].

Declaration of Competing Interest

The authors declare no conflict of interest.

Acknowledgement

The authors are thankful to SIC Facility at IIT Indore for NMR and CD experiments. N.J. and A.J. acknowledges the Council for Scientific and Industrial Research, Govt. of India, New Delhi, S.K.M acknowledges University Grant Commission, Govt. of India, New Delhi and U.S. acknowledges Ministry of Human Resource and Development, Govt. of India, New Delhi for Ph.D. research fellowships.

Appendix A. Supplementary data

Supplementary data to this article can be found online at https://doi.org/10.1016/j.ygeno.2020.09.010.

References

[1] M.A. Echeita, A. Aladuena, S. Cruchaga, M.A. Usera, Emergence and spread of an atypical *Salmonella enterica subsp. enterica* serotype 4,5,12:i:- strain in Spain, J. Clin. Microbiol. 37 (1999) 3425.
[2] F.W. Brenner, R.G. Villar, F.J. Angulo, R. Tauxe, B. Swaminathan, Salmonella Nomenclature, J. Clin. Microbiol. 38 (2000) 2465–2467.
[3] O. Gal-Mor, E.C. Boyle, G.A. Grassl, Same species, different diseases: how and why typhoidal and non-typhoidal *Salmonella enterica* serovars differ, Front. Microbiol. 5 (2014).
[4] J.A. Crump, S.P. Luby, E.D. Mintz, The global burden of typhoid fever, Bull. World Health Organ. 82 (2004) 346–353.
[5] S. Omulo, S.M. Thumbi, M.K. Njenga, D.R. Call, A review of 40 years of enteric antimicrobial resistance research in eastern Africa: what can be done better? Antimicrob Resist Infect Control 4 (2015) 1.
[6] A. Karkey, G.E. Thwaites, S. Baker, The evolution of anti-microbial resistance in Salmonella Typhi, Curr. Opin. Gastroenterol. 34 (2018) 25–30.
[7] S.-K. Eng, P. Pusparajah, N.-S. Ab Mutalib, H.-L. Ser, K.-G. Chan, L.-H. Lee, Salmonella: a review on pathogenesis, epidemiology and antibiotic resistance, Front. Life Sci. 8 (2015) 284–293.
[8] S. Chamnongpol, E.A. Groisman, Mg2+ homeostasis and avoidance of metal toxicity, Mol. Microbiol. 44 (2002) 561–571.
[9] T.J. Bourret, L. Liu, J.A. Shaw, M. Husain, A. Vazquez-Torres, Magnesium homeostasis protects Salmonella against nitrooxidative stress, Sci. Rep. 7 (2017) 15083.
[10] E.S. Sattely, M.A. Fischbach, C.T. Walsh, Total biosynthesis: in vitro reconstitution of polyketide and nonribosomal peptide pathways, Nat. Prod. Rep. 25 (2008) 757–793.
[11] K.N. Raymond, E.A. Dertz, S.S. Kim, Enterobactin: an archetype for microbial iron transport, Proc. Natl. Acad. Sci. U. S. A. 100 (2003) 3584–3588.
[12] S. Lun, H. Guo, J. Adamson, J.S. Cisar, T.D. Davis, S.S. Chavadi, J.D. Warren, L.E. Quadri, D.S. Tan, W.R. Bishai, Pharmacokinetic and in vivo efficacy studies of the mycobactin biosynthesis inhibitor salicyl-AMS in mice, Antimicrob. Agents Chemother. 57 (2013) 5138–5140.
[13] M. Balhara, R. Chaudhary, S. Ruhil, B. Singh, N. Dahiya, V.S. Parmar, P.K. Jaiwal, A.K. Chhillar, Siderophores; iron scavengers: the novel & promising targets for pathogen specific antifungal therapy, Expert Opin. Ther. Targets 20 (2016) 1477–1489.
[14] K.L. Stirrett, J.A. Ferreras, V. Jayaprakash, B.N. Sinha, T. Ren, L.E. Quadri, Small molecules with structural similarities to siderophores as novel anti-microbials against mycobacterium tuberculosis and Yersinia pestis, Bioorg. Med. Chem. Lett. 18 (2008) 2662–2668.
[15] F. Imperi, F. Massai, M. Facchini, E. Frangipani, D. Visaggio, L. Leoni, A. Bragonzi, P. Visca, Repurposing the antimycotic drug flucytosine for suppression of Pseudomonas aeruginosa pathogenicity, Proc. Natl. Acad. Sci. U. S. A. 110 (2013) 7458–7463.
[16] A.L. Lamb, Breaking a pathogen's iron will: inhibiting siderophore production as an anti-microbial strategy, Biochim. Biophys. Acta 1854 (2015) 1054–1070.
[17] M.L. Daus, M. Grote, E. Schneider, The MalF P2 loop of the ATP-binding cassette transporter MalFGK2 from Escherichia coli and Salmonella enterica serovar typhimurium interacts with maltose binding protein (MalE) throughout the catalytic cycle, J. Bacteriol. 191 (2009) 754–761.
[18] A. Vikram, G.K. Jayaprakasha, P.R. Jesudhasan, S.D. Pillai, B.S. Patil, Obacunone represses Salmonella pathogenicity islands 1 and 2 in an envZ-dependent fashion, Appl. Environ. Microbiol. 78 (2012) 7012–7022.
[19] J.L. Huppert, Four-stranded nucleic acids: structure, function and targeting of G-quadruplexes, Chem. Soc. Rev. 37 (2008) 1375–1384.
[20] E. Largy, A. Marchand, S. Amrane, V.R. Gabelica, J.-L. Mergny, Quadruplex turncoats: cation-dependent folding and stability of quadruplex-DNA double switches, J. Am. Chem. Soc. 138 (2016) 2780–2792.
[21] S. Balasubramanian, S. Neidle, G-quadruplex nucleic acids as therapeutic targets, Curr. Opin. Chem. Biol. 13 (2009) 345–353.
[22] B. Gatto, M. Palumbo, C. Sissi, Nucleic acid aptamers based on the G-quadruplex structure: therapeutic and diagnostic potential, Curr. Med. Chem. 16 (2009) 1248–1265.
[23] P. Murat, S. Balasubramanian, Existence and consequences of G-quadruplex structures in DNA, Curr. Opin. Genet. Dev. 25 (2014) 22–29.
[24] P. Rawal, V.B. Kummarasetti, J. Ravindran, N. Kumar, K. Halder, R. Sharma,

M. Mukerji, S.K. Das, S. Chowdhury, Genome-wide prediction of G4 DNA as regulatory motifs: role in Escherichia coli global regulation, Genome Res. 16 (2006) 644–655.
[25] E.P. Calvo, M. Wasserman, G-Quadruplex ligands: potent inhibitors of telomerase activity and cell proliferation in plasmodium falciparum, Mol. Biochem. Parasitol. 207 (2016) 33–38.
[26] B.D. Griffin, H.W. Bass, Review: plant G-quadruplex (G4) motifs in DNA and RNA; abundant, intriguing sequences of unknown function, Plant Sci. 269 (2018) 143–147.
[27] E. Ruggiero, S.N. Richter, G-quadruplexes and G-quadruplex ligands: targets and tools in antiviral therapy, Nucleic Acids Res. 46 (2018) 3270–3283.
[28] L.M. Harris, C.J. Merrick, G-quadruplexes in pathogens: a common route to virulence control? PLoS Pathog. 11 (2015) e1004562.
[29] J. Guillon, A. Cohen, R.N. Das, C. Boudot, N.M. Gueddouda, S. Moreau, L. Ronga, S. Savrimoutou, L. Basmaciyan, C. Tisnerat, Design, synthesis, and antiprotozoal evaluation of new 2, 9-bis [(substituted-aminomethyl) phenyl]-1, 10-phenanthroline derivatives, Chem. Biol. Drug Des. 91 (2018) 974–995.
[30] P. Majee, U. Shankar, S. Pasadi, K. Muniyappa, D. Nayak, A. Kumar, Genome-wide analysis reveals a regulatory role for G-quadruplexes during adenovirus multiplication, Virus Res. 197960 (2020).
[31] P. Majee, S. Kumar Mishra, N. Pandya, U. Shankar, S. Pasadi, K. Muniyappa, D. Nayak, A. Kumar, Identification and characterization of two conserved G-quadruplex forming motifs in the Nipah virus genome and their interaction with G-quadruplex specific ligands, Sci. Rep. 10 (2020) 1477.
[32] N. Beaume, R. Pathak, V.K. Yadav, S. Kota, H.S. Misra, H.K. Gautam, S. Chowdhury, Genome-wide study predicts promoter-G4 DNA motifs regulate selective functions in bacteria: radioresistance of D. radiodurans involves G4 DNA-mediated regulation, Nucleic Acids Res. 41 (2013) 76–89.
[33] Z.A. Waller, B.J. Pinchbeck, B.S. Buguth, T.G. Meadows, D.J. Richardson, A.J. Gates, Control of bacterial nitrate assimilation by stabilization of G-quadruplex DNA, Chem. Commun. (Camb.) 52 (2016) 13511–13514.
[34] S. Burge, G.N. Parkinson, P. Hazel, A.K. Todd, S. Neidle, Quadruplex DNA: sequence, topology and structure, Nucleic Acids Res. 34 (2006) 5402–5415.
[35] M. Vorlickova, I. Kejnovska, J. Sagi, D. Renciuk, K. Bednarova, J. Motlova, J. Kypr, Circular dichroism and Guanine quadruplexes, Methods (San Diego, Calif.) 57 (2012) 64–75.
[36] L. Oganesian, I.K. Moon, T.M. Bryan, M.B. Jarstfer, Extension of G-quadruplex DNA by ciliate telomerase, EMBO J. 25 (2006) 1148–1159.
[37] S. Artusi, M. Nadai, R. Perrone, M.A. Biasolo, G. Palù, L. Flamand, A. Calistri, S.N. Richter, The herpes simplex Virus-1 genome contains multiple clusters of repeated G-quadruplex: implications for the antiviral activity of a G-quadruplex ligand, Antivir. Res. 118 (2015) 123–131.
[38] S.R. Wang, Y.Q. Min, A Highly Conserved G-rich Consensus Sequence in Hepatitis C Virus Core Gene Represents a New Anti-Hepatitis C Target, 2 (2016) (e1501535).
[39] P. Murat, J. Zhong, L. Lekieffre, N.P. Cowieson, J.L. Clancy, T. Preiss, S. Balasubramanian, R. Khanna, J. Tellam, G-quadruplexes regulate Epstein-Barr virus-encoded nuclear antigen 1 mRNA translation, Nat. Chem. Biol. 10 (2014) 358–364.
[40] R. Perrone, E. Lavezzo, E. Riello, R. Manganelli, G. Palu, Mapping and Characterization of G-Quadruplexes in *Mycobacterium tuberculosis* Gene Promoter Regions, 7 (2017), p. 5743.
[41] U. Shankar, N. Jain, S.K. Mishra, T.K. Sharma, A. Kumar, Conserved G-quadruplex Motifs in gene promoter region reveals a novel therapeutic approach to target multi-drug resistance *Klebsiella pneumoniae*, Front. Microbiol. 11 (2020).
[42] R. Ferreira, A. Aviñó, S. Mazzini, R. Eritja, Synthesis, DNA-binding and antiproliferative properties of acridine and 5-methylacridine derivatives, Molecules 17 (2012) 7067–7082.
[43] R.J. Harrison, J. Cuesta, G. Chessari, M.A. Read, S.K. Basra, A.P. Reszka, J. Morrell, S.M. Gowan, C.M. Incles, F.A. Tanious, W.D. Wilson, L.R. Kelland, S. Neidle, Trisubstituted Acridine derivatives as potent and selective telomerase inhibitors, J. Med. Chem. 46 (2003) 4463–4476.
[44] S.R. Liao, C.X. Zhou, W.B. Wu, T.M. Ou, J.H. Tan, D. Li, L.Q. Gu, Z.S. Huang, 12-N-methylated 5,6-dihydrobenzo[c]acridine derivatives: a new class of highly selective ligands for c-myc G-quadruplex DNA, Eur. J. Med. Chem. 53 (2012) 52–63.
[45] Q.-L. Guo, H.-F. Su, N. Wang, S.-R. Liao, Y.-T. Lu, T.-M. Ou, J.-H. Tan, D. Li, Z.-S. Huang, Synthesis and evaluation of 7-substituted-5,6-dihydrobenzo[c]acridine derivatives as new c-KIT promoter G-quadruplex binding ligands, Eur. J. Med. Chem. 130 (2017) 458–471.
[46] A. Tawani, A. Amanullah, A. Mishra, A. Kumar, Evidences for Piperine inhibiting cancer by targeting human G-quadruplex DNA sequences, Sci. Rep. 6 (2016) 39239.
[47] A. Tawani, S.K. Mishra, A. Kumar, Structural insight for the recognition of G-quadruplex structure at human c-myc promoter sequence by flavonoid Quercetin, Sci. Rep. 7 (2017) 3600.
[48] T. Endoh, Y. Kawasaki, N. Sugimoto, Suppression of gene expression by G-quadruplexes in open reading frames depends on G-quadruplex stability, Angew. Chem. Int. Ed. Eng. 52 (2013) 5522–5526.
[49] S.R. Wang, Q.Y. Zhang, J.Q. Wang, X.Y. Ge, Y.Y. Song, Y.F. Wang, X.D. Li, B.S. Fu, G.H. Xu, B. Shu, P. Gong, B. Zhang, T. Tian, X. Zhou, Chemical targeting of a G-Quadruplex RNA in the Ebola virus L gene, Cell Chem. Biol. 23 (2016) 1113–1122.
[50] T. Endoh, Y. Kawasaki, N. Sugimoto, Stability of RNA quadruplex in open reading frame determines proteolysis of human estrogen receptor alpha, Nucleic Acids Res. 41 (2013) 6222–6231.
[51] D. Monchaud, M.-P. Teulade-Fichou, A hitchhiker's guide to G-quadruplex ligands, Org. Biomol. Chem. 6 (2008) 627–636.
[52] J.-L. Li, R.J. Harrison, A.P. Reszka, R.M. Brosh, V.A. Bohr, S. Neidle, I.D. Hickson, Inhibition of the Bloom's and Werner's syndrome helicases by G-Quadruplex interacting ligands, Biochemistry 40 (2001) 15194–15202.
[53] S.-R. Liao, C.-X. Zhou, W.-B. Wu, T.-M. Ou, J.-H. Tan, D. Li, L.-Q. Gu, Z.-S. Huang, 12-N-methylated 5,6-dihydrobenzo[c]acridine derivatives: a new class of highly selective ligands for c-myc G-quadruplex DNA, Eur. J. Med. Chem. 53 (2012) 52–63.
[54] M. Read, R.J. Harrison, B. Romagnoli, F.A. Tanious, S.H. Gowan, A.P. Reszka, W.D. Wilson, L.R. Kelland, S. Neidle, Structure-based design of selective and potent G quadruplex-mediated telomerase inhibitors, Proc. Natl. Acad. Sci. 98 (2001) 4844–4849.
[55] M. Laronze-Cochard, Y.-M. Kim, B. Brassart, J.-F. Riou, J.-Y. Laronze, J. Sapi, Synthesis and biological evaluation of novel 4,5-bis(dialkylaminoalkyl)-substituted acridines as potent telomeric G-quadruplex ligands, Eur. J. Med. Chem. 44 (2009) 3880–3888.
[56] M.J.B. Moore, C.M. Schultes, J. Cuesta, F. Cuenca, M. Gunaratnam, F.A. Tanious, W.D. Wilson, S. Neidle, Trisubstituted acridines as G-quadruplex telomere targeting agents. Effects of extensions of the 3,6- and 9-side chains on quadruplex binding, telomerase activity, and cell proliferation, J. Med. Chem. 49 (2006) 582–599.
[57] C. Bazzicalupi, M. Chioccioli, C. Sissi, E. Porcù, C. Bonaccini, C. Pivetta, A. Bencini, C. Giorgi, B. Valtancoli, F. Melani, P. Gratteri, Modeling and biological investigations of an unusual behavior of novel synthesized Acridine-based polyamine ligands in the binding of double Helix and G-Quadruplex DNA, ChemMedChem 5 (2010) 1995–2005.
[58] R. Ferreira, R. Artali, A. Benoit, R. Gargallo, R. Eritja, D.M. Ferguson, Y.Y. Sham, S. Mazzini, Structure and stability of human Telomeric G-Quadruplex with preclinical 9-amino Acridines, PLoS One 8 (2013) e57701.
[59] S.K. Mishra, A. Tawani, A. Mishra, A. Kumar, G4IPDB: a database for G-quadruplex structure forming nucleic acid interacting proteins, Sci. Rep. 6 (2016) 38144.
[60] O. Kikin, L. D'Antonio, P.S. Bagga, QGRS mapper: a web-based server for predicting G-quadruplexes in nucleotide sequences, Nucleic Acids Res. 34 (2006) W676–W682.
[61] J. Hon, T. Martinek, J. Zendulka, M. Lexa, pqsfinder: an exhaustive and imperfection-tolerant search tool for potential quadruplex-forming sequences in R, Bioinformatics (Oxford, England) 33 (2017) 3373–3379.
[62] T.L. Bailey, M. Boden, F.A. Buske, M. Frith, C.E. Grant, L. Clementi, J. Ren, W.W. Li, W.S. Noble, MEME SUITE: tools for motif discovery and searching, Nucleic Acids Res. 37 (2009) W202–W208.
[63] C. Valgas, S.M.D. Souza, E.F. Smânia, A. Smânia Jr., Screening methods to determine anti-bacterial activity of natural products, Braz. J. Microbiol. 38 (2007) 369–380.
[64] J. Wang, H. Liu, J. Zhao, H. Gao, L. Zhou, Z. Liu, Y. Chen, P. Sui, Anti-microbial and antioxidant activities of the root bark essential oil of Periploca sepium and its main component 2-hydroxy-4-methoxybenzaldehyde, Molecules 15 (2010) 5807–5817.
[65] S.K. Mishra, N. Jain, U. Shankar, A. Tawani, T.K. Sharma, A. Kumar, Characterization of highly conserved G-quadruplex motifs as potential drug targets in Streptococcus pneumoniae, Sci. Rep. 9 (2019) 1791.